Pergamon

Geochimica et Cosmochimica Acta, Vol. 67, No. 11, pp. 2063–2076, 2003

0016-7037/03 $30.00 + .00

doi:10.1016/S0016-7037(02)01299-1

Synthesis, characterization, and thermochemistry of K-Na-H_3O jarosites

CHRISTOPHE DROUET and ALEXANDRA NAVROTSKY*

Thermochemistry Facility, Department of Chemical Engineering and Materials Science, University of California at Davis, One Shields Avenue, Davis, CA 95616, USA

(*Received May* 24, 2002; *accepted in revised form October* 7, 2002)

Abstract—The thermochemistry of well-characterized synthetic K-H_3O, Na-H_3O and K-Na-H_3O jarosites was investigated. These phases are solid solutions that obey Vegard's law. Electron probe microanalyses indicated lower alkali and iron contents than predicted from the theoretical end-member compositions, in agreement with thermal analyses, suggesting the presence of hydronium and "additional" water. The standard enthalpies of formation ($\Delta H°_f$) of K-H_3O, Na-H_3O and K-Na-H_3O jarosites were determined by high-temperature oxide melt solution calorimetry. These enthalpies vary linearly with the K/H_3O, Na/H_3O and K/Na ratio, respectively. The enthalpy of formation of pure hydronium jarosite was also determined experimentally ($\Delta H°_f = -3741.6 \pm 8.3$ kJ.mol^{-1}), and it was used to evaluate $\Delta H°_f$ for the end-members $KFe_3(SO_4)_2(OH)_6$ ($\Delta H°_f = -3829.6 \pm 8.3$ kJ.mol^{-1}) and $NaFe_3(SO_4)_2(OH)_6$ ($\Delta H°_f = -3783.4 \pm 8.3$ kJ.mol^{-1}). Finally, enthalpies of dehydration (loss of the "additional" water) of some jarosites were determined and found to be near the enthalpy of vaporization of water, suggesting that the "additional" water is weakly bonded in the structure. *Copyright © 2003 Elsevier Science Ltd*

1. INTRODUCTION

Jarosites are hydrous sulfate minerals containing alkalis and ferric iron. Especially during the past few decades, they have received increasing attention in many geologic, environmental, and industrial fields. Despite this interest, there is a lack of thermodynamic data.

Jarosites are frequently observed in sulfate-rich environments such as acid sulfate soils formed from sulfide sediments, acid mine drainage, and weathering of sulfide ore deposits. The dissolution of jarosites can generate high concentrations of sulfate ion in waters draining such sites, which raises environmental concerns (Alpers et al., 1989). The precipitation of jarosite can also be exploited intentionally, as in zinc hydrometallurgy, where jarosites are used to efficiently remove iron impurities (Arregiu et al., 1979; Dutrizac, 1979; Dutrizac and Jambor, 1984).

Natural jarosites are indicators of paleoclimatic conditions (Arehart and O'Neil, 1993; Rye et al., 1993; Vasconcelos et al., 1994). Prehistoric Native American cultures used jarosites as paint pigments (Kay et al., 1996). Recently, some spectral features of Martian soil were attributed to jarosites, which raised interest within the planetary geology community (Burns, 1987; Ming et al., 1996). Also, jarosites are promising in the field of construction materials (Mymrin and Vaamonde, 1999).

Jarosites can be described by the idealized formula $AFe_3(SO_4)_2(OH)_6$. Whereas A most commonly stands for potassium (jarosite), sodium (natrojarosite), hydronium, or ammonium, other ions such as Tl^+, Pb^{2+}, or Ag^+ can be located in A-sites as well (Balic-Zunic et al., 1994; Breidenstein et al., 1992; Dutrizac, 1984). Also, iron can be substituted by other trivalent ions such as Al^{3+} (alunite), Ga^{3+}, or Cr^{3+} (Hendricks, 1937; Jambor et al., 1996; Lengauer et al., 1994). Substitution of sulfur by trace elements of environmental concern such as Cr^{6+} or As^{5+} also has been reported (Baron and Palmer, 1996b; Dutrizac et al., 1987).

Previous work on jarosites has focused mainly on their synthesis and crystallographic features (Menchetti and Sabelli, 1976). The structure of jarosite $KFe_3(SO_4)_2(OH)_6$ and alunite $KAl_3(SO_4)_2(OH)_6$ was investigated in detail by Hendricks (1937). Substitution of hydronium ions H_3O^+ for potassium or sodium in A-sites has been reported (Kubisz, 1970; Dutrizac and Kaiman, 1976; Ripmeester et al., 1986). Kubisz (1964) and Brophy and Sheridan (1965) showed that most of the natural jarosites were solid solutions of hydronium jarosite, sodium jarosite (also called natrojarosite), and potassium jarosite. Based on X-ray diffraction analyses, Brophy and Sheridan (1965) reported the existence of a complete K-Na-H_3O jarosite solid solution. These results were later confirmed by Herbert (1997). Discrepancies exist in the literature about the value of the unit cell parameters of K-, Na- and H_3O-jarosites, and Alpers et al. (1992) inferred that variations in the published data could be partly due to the presence of hydronium ions in A-sites, sometimes unsuspected by the authors.

Deficiencies in iron or aluminum have also been observed, both for natural and synthetic jarosites and alunites. As noted by Kubisz (1970), during the formation of natural jarosites, the source of iron and sulfur often is the decomposition of pyrite FeS_2, which results in Fe/S lower than in jarosite. Kubisz (1970) suggested that the incorporation of protons, most probably joining hydroxyl groups to form water molecules, could balance the lack of positive charge. Parker (1954) also mentioned the presence of "excess water" and trivalent ion deficiencies. Hendricks (1937) noted that water probably replaced hydroxyl groups randomly so that crystal symmetry was retained. Ripmeester et al. (1986) experimentally established from nuclear magnetic resonance studies that water molecules substitute for hydroxyl groups in alunite. Presumably similar substitution occurs in jarosite.

Although a few studies have addressed the thermochemistry of jarosites (see review in Baron and Palmer, 1996a), their

* Author to whom correspondence should be addressed (anavrotsky@ucdavis.edu).

thermodynamic properties are still poorly unknown. Potential-pH diagrams have been drawn (Brown, 1971; Van Breemen and Harmsen, 1975; Alpers et al., 1989; Stahl et al., 1993; Stoffregen, 1993) showing a boundary between jarosite and hematite (α–Fe_2O_3) around pH = 2 to 4 (jarosite being stable below this limit), and a stability field of goethite (FeOOH) above pH = 2 to 3. Attempts to evaluate the free energy of formation ($\Delta G°_f$) of jarosites were made. For calculations from dissolution studies, the end-member compositions were generally assumed a priori, and the establishment of equilibrium in solution was not always demonstrated (Brown, 1970; Zotov et al., 1973; Vlek et al., 1974; Kashkay et al., 1975; Stoffregen, 1993). By considering the most reliable data, Stoffregen et al. (2000) recommended values for the free energy of formation from the elements at 298 K as $\Delta G°_f = -3309.8$ kJ.mol^{-1} (Baron and Palmer, 1996a) for potassium jarosite and $\Delta G°_f =$ –3256.7 kJ.mol^{-1} (Kashkay et al., 1975) for natrojarosite.

To our knowledge, no direct determination of the enthalpy of formation of jarosites has been published. From the data available, Stoffregen (1993) calculated for potassium jarosite $\Delta H°_f \approx -3715.1$ kJ.mol^{-1} from data on alunite, hematite, and corundum reported by Helgeson et al. (1978). Similarly, Stoffregen (1993) evaluated the enthalpy of formation of natrojarosite (–3673.1 kJ.mol^{-1}) and the standard entropy of jarosite (388.9 J.mol^{-1}.K^{-1}) and natrojarosite (382.4 J.mol^{-1}.K^{-1}).

The purpose of this work is, thus, to study the thermochemistry of well-characterized synthetic K-H_3O, Na-H_3O and K-Na-H_3O jarosites. Complementary techniques such as X-ray diffraction (XRD), electron probe microanalysis (EPMA), thermal analysis (thermo-gravimetry/differential scanning calorimetry, TG/DSC), and Fourier-transform infrared spectroscopy (FTIR) were used to characterize these compounds. Their enthalpies of formation were determined by high-temperature oxide melt solution calorimetry, and values of $\Delta H°_f$ for end-member compositions were derived. A consistent set of $\Delta H°_f$, $\Delta S°_f$, and $\Delta G°_f$ values at 25°C is recommended.

2. EXPERIMENTAL

2.1. Synthesis

Unless otherwise specified, the K-H_3O, Na-H_3O and K-Na-H_3O jarosites prepared in this work were synthesized by coprecipitation for 4 h at 95°C under constant stirring of 4.10 g of reagent grade iron (III) sulfate ($Fe_2(SO_4)_3$), dehydrated overnight at 110°C, with varying amounts of reagent grade K_2SO_4 and/or Na_2SO_4. Sulfuric acid was added to maintain 0.1 mol/L concentration, to prevent hydrolysis of Fe^{3+} (Brophy et al., 1962). The volume of the solution was 100 mL. Deionized water was added during the synthesis to compensate for evaporation. The precipitate was then allowed to settle, separated from the solution by filtration, washed several times with deionized water, and dried at 110°C overnight.

The pure hydronium jarosite end-member $(H_3O)Fe_3(SO_4)_2(OH)_6$ was synthesized hydrothermally in a sealed silica glass capsule at 140°C for 1 week. The initial amount of iron (III) sulfate was 500 mg, dissolved in 5 mL of deionized water. Some Na-H_3O jarosites have been synthesized by a similar hydrothermal route. In that case, the desired proportion of sodium sulfate was added in the initial solution.

Dehydrated jarosites were obtained by heating jarosite samples under argon at 10°C/min to 320°C and then cooling to room temperature. After cooling, the sample was placed in contact with atmospheric air and left to equilibrate for 12 h.

The compound $KFe_3(SO_4)(OH)_6$ will be referred as "potassium jarosite" rather than "jarosite." This underlines the occupation of the A-sites by potassium as opposed to sodium or hydronium.

2.2. Characterization

Powder X-ray diffraction (XRD) patterns were recorded with a Scintag PAD-V diffractometer operated at 45 kV and 40 mA and using Cu Kα radiation (λ = 1.54056 Å). The diffractometer was calibrated with quartz as a standard. The unit cell parameters were calculated by least square refinement based on the location and intensity of the peaks. For data collection and refinement, the software JADE, version 6.1, produced by Materials Data Inc. was used.

Quantitative elemental analyses were carried out with a Cameca SX-50 electron microprobe. Orthoclase $KAlSi_3O_8$, albite $NaAlSi_3O_8$, hematite α–Fe_2O_3, and calcium sulfate $CaSO_4$ were chosen as standards for K, Na, Fe, and S, respectively. The powdered samples were pressed into a 5-mg pellet and immobilized with epoxy resin. Scatter on each determination was ~5% as shown by the corresponding standard deviations. This value is somewhat higher than usual, possibly due to the major amounts of oxygen and hydrogen present, and to some difficulty in polishing these soft minerals. The microprobe results were used to determine the potassium, sodium, iron, and sulfur contents, per unit formula containing two sulfate groups, from the measured ratios (K + Na)/S and Fe/S. The hydronium content was then derived from the potassium and sodium contents using K + Na + H_3O = 1 (A-site substitutions). The amount of iron vacancies (z) was determined from the iron content (3−z), and this quantity was used to derive the OH and additional water contents using the chemical formula $(K)_{1-x-y}$ $(Na)_y$ $(H_3O)_x$ $(Fe)_{3-z}$ $(SO_4)_2$ $(OH)_{6-3z}$ $(H_2O)_{3z}$. This formula accounts for overall crystal neutrality in which z iron vacancies lead to a lack of 3z positive charges, which is then compensated by the protonation of 3z hydroxyl groups to give 3z water molecules. The water content 3z found here is supported by the good agreement seen between microprobe and TG results. In the text, each jarosite sample will be referred to as "K(u)Na(v)Fe(w)" where u, v, and w respectively represent the potassium, sodium, and iron molar content per formula unit.

Thermal analyses (TG/DSC) were performed on a Netzsch STA 449 C apparatus. The carrier gas was argon flowing at 50 mL/min. The heating rate was 10°C/min. Gases evolved during thermal analysis could be analyzed by FTIR (see below).

Differential scanning calorimetry (DSC) was used to determine the heat capacity. This was performed on a Netzsch 404 heat-flow DSC instrument. Cooling was provided by evaporating gaseous nitrogen. The sample was pelletized to ensure good thermal contact. A helium atmosphere with a flow rate of 40 mL/min was used.

FTIR spectra were collected with a Bruker EQUINOX 55 spectrometer using the KBr pellet technique. Pellets (13 mm diameter, 150 mg) were pressed under 300 bar for 1 min. The infrared (IR) spectra were recorded immediately after pellet preparation. The spectrometer was flushed continuously with nitrogen to avoid contamination of the pellet during the analysis. Spectra were collected in the 400 to 4000 cm^{-1} range with a resolution of 4 cm^{-1}. A baseline correction was made before interpretation.

2.3. High-temperature Calorimetry

High-temperature drop solution calorimetry was carried out at 700°C in a Tian-Calvet twin calorimeter, as described in detail by Navrotsky (1977, 1997). Sodium molybdate ($3Na_2O.\ 4MoO_3$) was the solvent.

Dissolution times in all cases were less than 1 h. The end of the reaction was judged by the return of the baseline to its initial value. During the experiments, oxygen was flushed through the gas space above the melt (~35 mL/min) and bubbled through the solvent (~5 mL/min) to maintain oxidizing conditions, stir the melt, and help remove the evolved water.

Sulfur remained in the solvent as no sulfur-containing gas was evolved during the dissolution of the samples in sodium molybdate. This point was evaluated in this work by dropping pellets of samples into a platinum crucible containing molten sodium molybdate solvent and analyzing the gases evolved by FTIR. This finding is comparable to the results obtained by Majzlan et al. (2002) for anhydrous sulfates. Also, a piece of pH paper, moistened with deionized water, was placed just above the crucible during the dissolution of the pellet in the solvent (in a simulated calorimetric experiment in a short furnace) and no acidity was observed, indicating the absence of H_2SO_4. As shown in earlier work (Navrotsky et al., 1994), the H_2O in such drop solution

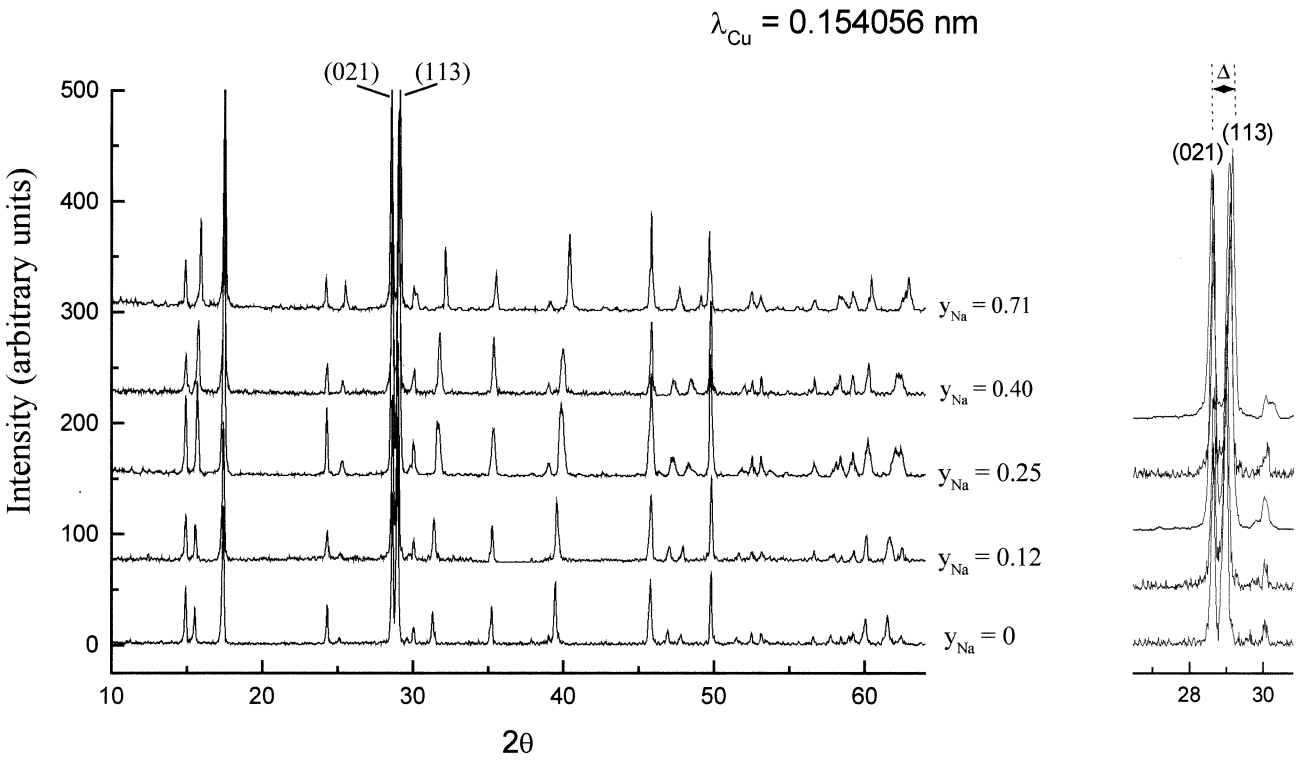

Fig. 1. Evolution of the X-ray diffraction pattern of ($K_{0.7-y}$, Na_y, $(H_3O)_{0.3}$) jarosites as a function of the sodium content.

experiments is released completely to the flowing gas atmosphere. Thus, the final state in these calorimetric experiments is a dilute solution in $3Na_2O$. $4MoO_3$ of the sulfates of Na, K, and Fe^{3+} (as ions in the melt) and gaseous H_2O, all at 700°C.

3. RESULTS AND DISCUSSION

3.1. Solid Characterization

3.1.1. X-ray diffraction and electron probe microanalysis

The heating at 95°C of an aqueous solution of potassium and iron sulfates under acidic conditions (0.1 mol/L H_2SO_4) led to the fast precipitation of a yellow phase (Munsell color 0.2 Y 7.9/4.7) easily identified by X-ray diffraction as jarosite by comparison with the diffraction pattern International Center for Diffraction Data-Power Diffraction File (ICDD PDF) No. 22-0827, corresponding to potassium jarosite. A typical X-ray diffraction pattern is shown in Figure 1 (sample $y_{Na} = 0$). No other crystalline phase was detected.

The unit cell parameters of potassium jarosites prepared from various initial iron/potassium ratios are reported in Table 1. Unit cell parameters "a" and "c" are near 7.31 Å and 17.10 Å respectively, intermediate between those reported for K-jarosite and H_3O-jarosite (Alpers et al., 1992).

For all samples, the atomic percentages of potassium and iron were less than theoretical values for the formula $KFe_3(SO_4)_2(OH)_6$, indicating a possible substitution of part of the K^+ and OH^- ions by H_3O^+ and H_2O respectively, in accord with literature results (Kubisz, 1970; Dutrizac and Kaiman, 1976; Ripmeester et al., 1986). Potassium jarosites synthesized here are, thus, K-H_3O jarosites. Their corresponding chemical compositions are given in Table 1. Even when using an excess of K_2SO_4, the jarosite phases formed by this coprecipitation method contain a significant amount of hydronium ions. These findings can be compared to those of Dutrizac and Jambor (1984) who synthesized solid solutions of silver jarosite and lead jarosite but did not obtain the end-member compositions due to residual hydronium.

Another synthesis route was investigated to try to reach the K-jarosite end-member composition. This method was based on the coprecipitation of 5.60 g of KOH (excess) and 14 g of anhydrous iron (III) sulfate in 100 mL of water. Kubisz (1970) reported that introduction of the alkalis as hydroxides could improve the sulfate-to-iron ratio in the precipitated jarosites. Baron and Palmer (1996a) reported the preparation of potassium jarosites close to the end-member composition using this method. The synthesis process was then continued as above. The phase obtained was identified as jarosite by X-ray diffraction, with a pattern similar to that of pure potassium jarosite. The unit cell parameters were a = 7.308 ± 0.0008 Å and c = 17.155 ± 0.001 Å, which are near to the published values (a = 7.29 Å and c = 17.16 Å, ICDD PDF No. 22-0827). Microprobe analyses showed, however, that the iron and potassium contents per unit formula were still somewhat less than three and one, respectively, leading to the composition ($K_{0.86}$ $H_3O_{0.14}$)$Fe_{2.69}(SO_4)_2(OH_{5.07}$ $H_2O_{0.93}$).

Sodium jarosite was synthesized through the coprecipitation of sodium sulfate and iron (III) sulfate in a similar way. Again, a jarosite crystalline phase (yellow, Munsell color 3.0 Y 7.6/5.6) was produced regardless of the initial iron/sodium ratio

Table 1. Unit cell parameters of the jarosites synthesized in this work.

Jarosite	Initial mass (g)			Unit cell parameters	
	$Fe_2(SO_4)_3$	K_2SO_4	Na_2SO_4	a (Å)	c (Å)
a) Potassium jarosites					
K(0.86)Na(0)Fe(2.69)[a]	—	—	—	7.308 ± 0.001	17.155 ± 0.001
K(0.72)Na(0)Fe(2.60)	4.10	0.70	0	7.321 ± 0.002	17.057 ± 0.004
K(0.68)Na(0)Fe(2.58)	4.10	0.50	0	7.318 ± 0.002	17.133 ± 0.005
K(0.67)Na(0)Fe(2.68)	4.10	0.10	0	7.319 ± 0.001	17.084 ± 0.003
K(0.64)Na(0)Fe(2.82)	4.10	0.03	0	—	—
K(0.58)Na(0)Fe(2.48)	4.10	1.74	0	7.304 ± 0.001	17.060 ± 0.003
K(0.28)Na(0)Fe(2.52)	4.10	0.87	0	7.312 ± 0.002	17.027 ± 0.004
b) Sodium jarosites					
K(0)Na(0.82)Fe(2.91)[b]	0.50	0	0.06	—	—
K(0)Na(0.71)Fe(2.63)	4.10	0	2.13	7.335 ± 0.001	16.671 ± 0.003
K(0)Na(0.68)Fe(2.83)	4.10	0	1.20	—	—
K(0)Na(0.61)Fe(2.86)	4.10	0	0.80	—	—
c) Potassium-Sodium jarosites					
K(0.63)Na(0.08)Fe(2.57)	4.10	0.50	2.13	7.324 ± 0.003	17.003 ± 0.006
K(0.59)Na(0.12)Fe(2.59)	4.10	0.30	2.13	7.317 ± 0.001	17.069 ± 0.004
K(0.47)Na(0.25)Fe(2.64)	4.10	0.10	2.13	7.327 ± 0.002	16.968 ± 0.008
K(0.43)Na(0.29)Fe(2.66)	4.10	0.06	2.13	7.324 ± 0.001	16.971 ± 0.007
K(0.33)Na(0.40)Fe(2.67)	4.10	0.03	2.13	7.325 ± 0.001	16.880 ± 0.007

[a] From coprecipitation of KOH and iron (III) sulfate.
[b] From hydrothermal synthesis.

(Table 1). Each X-ray diffraction pattern showed that the only phase present was natrojarosite (pattern ICDD PDF No. 36-0425). The yield of the reaction decreased strongly with decrease in initial mass of sodium sulfate, which limited us to using more than 0.80 g of Na_2SO_4.

Electron microprobe analyses showed that the sodium and iron contents were low, indicating the partial substitution of Na^+ by H_3O^+ and the presence of iron vacancies. Consequently, these phases will be referred to as Na-H_3O jarosites. The unit cell parameters for K(0)Na(0.71)Fe(2.63) were a = 7.335 ± 0.001 Å and c = 16.671 ± 0.003 Å. These values are near to those reported by Dutrizac and Kaiman (1976) for natrojarosite.

The existence of a complete K-Na-H_3O jarosite solid solution has been reported (Brophy and Sheridan, 1965). Therefore, the coprecipitation of K_2SO_4, Na_2SO_4, and $Fe_2(SO_4)_3$ was investigated here, using the same conditions as above. Again, only a jarosite phase was observed by X-ray diffraction. The experimental patterns obtained with varying Fe/K/Na amounts were intermediate between the patterns of potassium jarosite and natrojarosite.

Electron microprobe analyses are reported in Table 1. A family of compounds containing ~0.3 mol of H_3O^+ cations per formula unit can be distinguished. The members of this series will be referred to as ($K_{0.7-y}$ Na_y $(H_3O)_{0.3}$) jarosites. The composition of these compounds resembles the average composition (molar content of 0.25 for H_3O^+ and between 3.00 and 2.60 for Fe^{3+}) determined by Kubisz (1970) from the analysis of 40 jarosite samples synthesized at low temperature. Alpers et al. (1989) also have reported hydronium contents between 0.10 and 0.32 for K-Na-H_3O jarosite solid solutions.

The X-ray diffraction patterns obtained for the phases corresponding to y_{Na} = 0, 0.12, 0.25, 0.40, and 0.71 are shown in Figure 1. Their gradual evolution is consistent with the existence of a continuous solid solution. For the ($K_{0.7-y}$ Na_y $(H_3O)_{0.3}$) jarosite series, the unit cell parameter "c" varies from 17.069 ± 0.004 Å to 16.671 ± 0.003 Å with increasing y_{Na}, whereas the parameter "a" remains almost constant (Table 1). These values are consistent with the jarosite structure and ionic radii involved (r_{K+} = 1.64 Å, r_{Na+} = 1.39 Å; Shannon and Prewitt, 1969; Shannon, 1976), and are in agreement with results published by Brophy and Sheridan (1965) and Alpers et al. (1992). Parker (1962) showed that substitution of potassium by sodium in alunite led to little change in the parameter "a" but to a marked decrease in "c." The unit cell parameters and volume are plotted in Figure 2 as a function of the sodium content. Although there are slight variations in the iron and hydronium contents among the samples, linear relations are seen, in accord with Vegard's law, consistent with solid solution formation. A linear variation of the parameter "c" was also reported by Stoffregen and Alpers (1992) for the alunite-natroalunite solid solutions.

3.1.2. Thermal analysis

The thermal decomposition of the jarosites synthesized in this work has been investigated by TG/DSC analyses performed under argon up to 1000°C. Similar profiles were obtained for all jarosites tested, although variations in the position and intensity of some peaks were observed. Typical TG and DSC curves obtained with a K-H_3O jarosite (sample K(0.86)Na(0)Fe(2.69)) are given in Figure 3. Samples with high sodium contents showed an additional endothermic peak around 890°C due to the melting of Na_2SO_4 produced.

Several weight loss events are seen. The DSC curve shows two intense endothermic peaks and a series of weaker endothermic and exothermic peaks, in agreement with earlier results (Kulp and Adler, 1950; Alías and Girella, 1968; Kubisz, 1971; Kashkay et al., 1975). X-ray diffraction analyses were per-

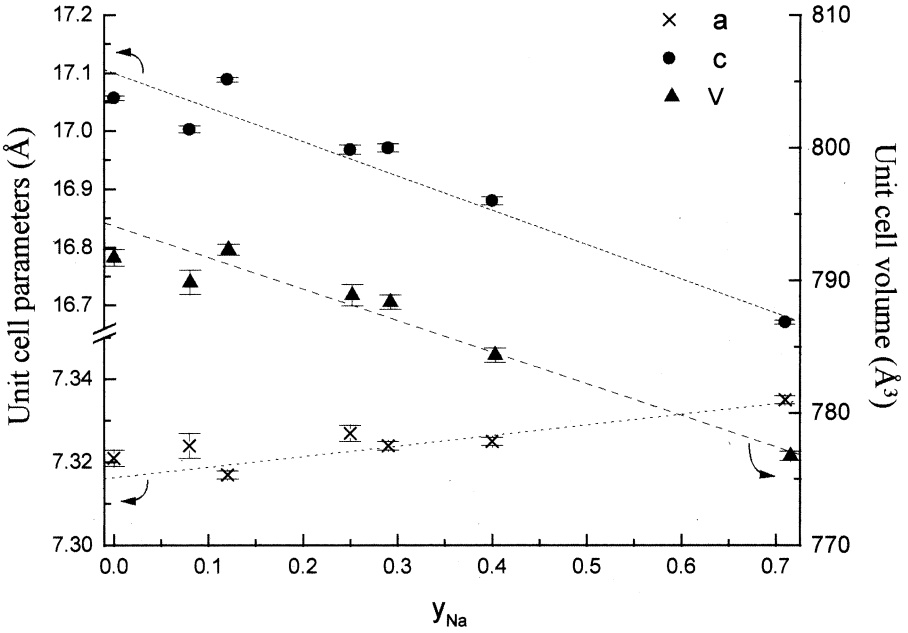

Least square refinement Y = A + B . X	A	B	R^2
Unit cell parameter "a":	7.316 ± 0.002	0.025 ± 0.004	0.933
Unit cell parameter "c":	17.100 ± 0.025	-0.590 ± 0.058	0.977
Unit cell volume "V":	794.09 ± 0.87	-23.96 ± 1.98	0.983

Fig. 2. Variation of the unit cell volume and unit cell parameters of ($K_{0.7-y}$, Na_y, $(H_3O)_{0.3}$) jarosites as a function of the sodium content.

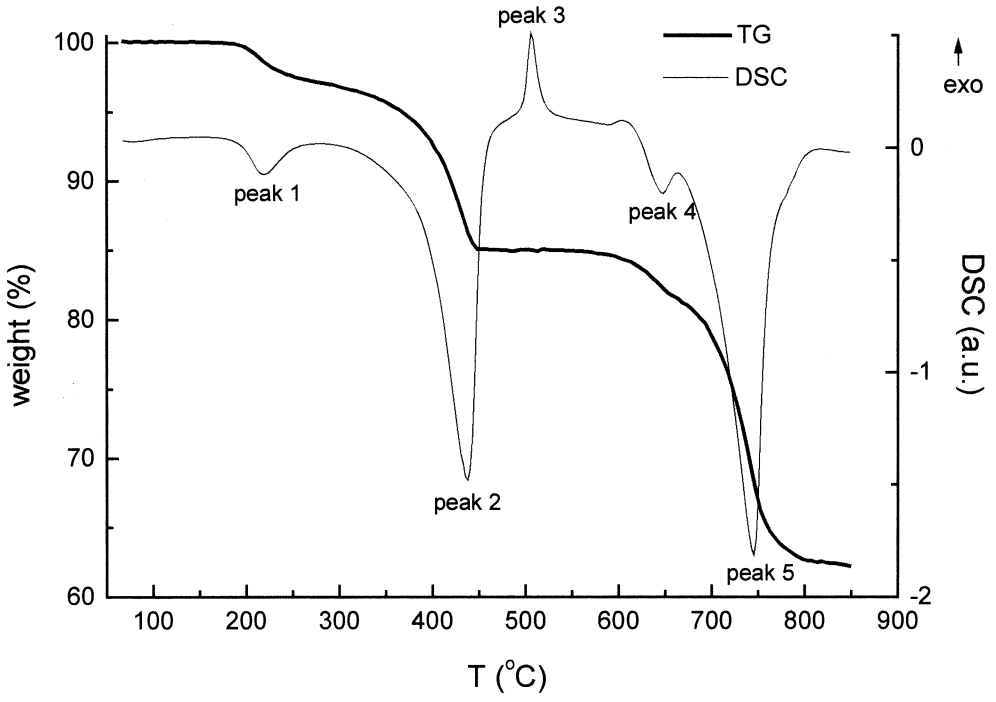

Fig. 3. TG and DSC curves for the jarosite K(0.86)Na(0)Fe(2.69) heated under argon up to 900°C.

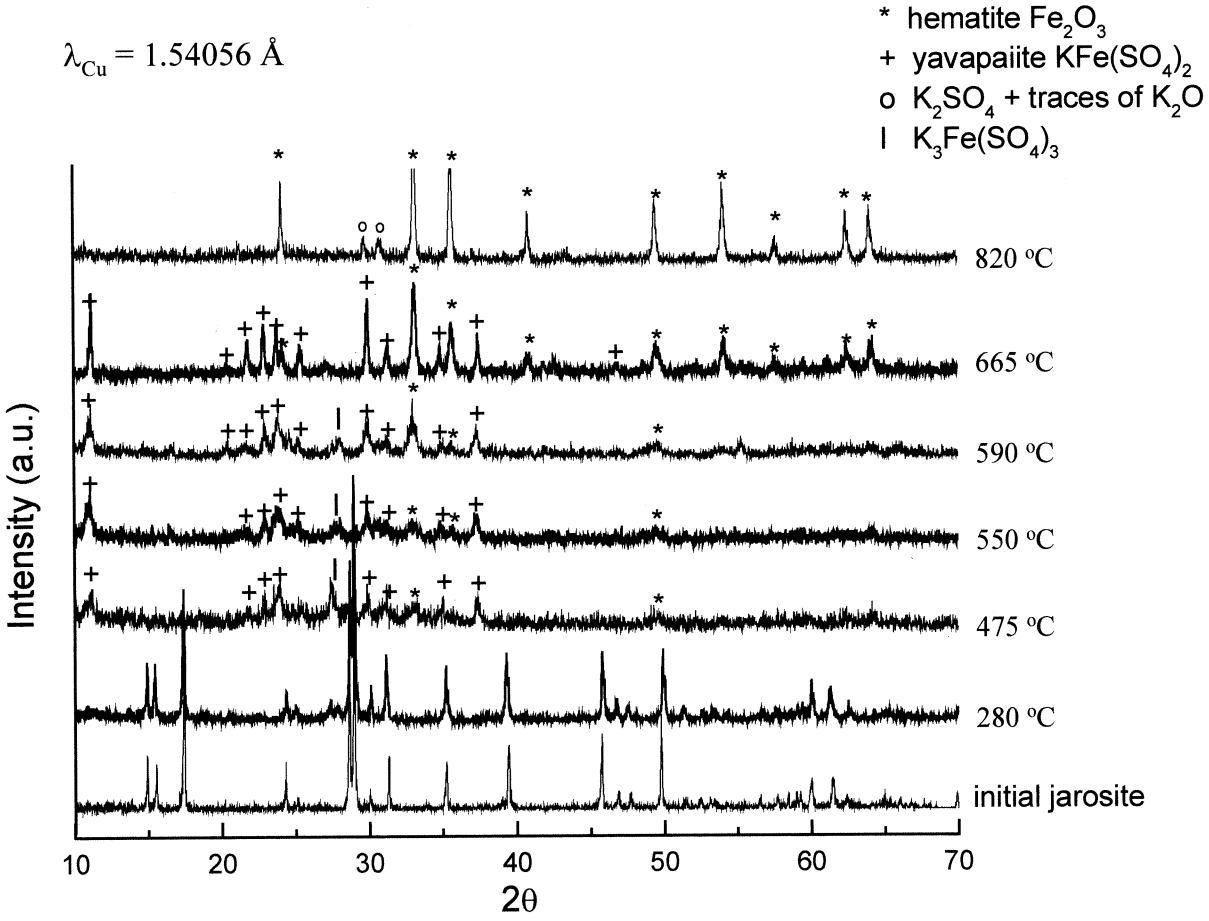

Fig. 4. X-ray diffraction patterns for the thermal decomposition of the jarosite K(0.86)Na(0)Fe(2.69) under argon.

formed after heating the samples under argon to various relevant temperatures selected from the TG/DSC profiles (Fig. 4).

The maximum of the first endothermic peak (labeled peak 1 in Fig. 3) was observed at 220°C for K(0.86)Na(0)Fe(2.69) and 250°C for K(0)Na(0.71)Fe(2.63). It has been attributed to the loss of H_2O molecules referred to as "additional" water (Kubisz, 1971). Infrared spectroscopy indicates that water vapor is the only evolved gas detected at these temperatures.

Table 2. Amount of "additional" water per unit formula determined from electron probe microanalysis and TG analysis.

	Amount of "additional" water (mole per unit formula)	
	From microprobe[a]	From TG
K(0.72)Na(0)Fe(2.60)	1.20	1.32
K(0.68)Na(0)Fe(2.58)	1.26	1.28
K(0.63)Na(0.08)Fe(2.57)	1.29	1.33
K(0.59)Na(0.12)Fe(2.59)	1.23	0.98
K(0.47)Na(0.25)Fe(2.64)	1.08	1.04
K(0.43)Na(0.29)Fe(2.66)	1.02	1.00
K(0.19)Na(0.51)Fe(2.77)	0.69	0.88
K(0)Na(0.71)Fe(2.63)	1.11	1.01

[a] Retained values.

X-ray diffraction shows that the jarosite structure is essentially preserved at 280°C (Fig. 4), as only traces of another phase, $K_3Fe(SO_4)_3$, were observed (one major line at the angle $2\theta \approx 27.0°$, line (212), ICDD PDF No. 30-0943). This phase probably is formed by a slight dehydroxylation of the jarosite.

When a jarosite is heated at 280°C a second time (after cooling and equilibrating with atmospheric air), no further weight loss is observed, showing that the jarosite structure persists after elimination of the "additional" water. This is similar to the results obtained by Brophy et al. (1962). The heated and unheated samples have similar lattice parameters.

From the weight loss corresponding to peak 1 (Fig. 3), the amount of "additional" water can be estimated and compared to the electron microprobe results (Table 2). There is good agreement between both sets of data.

The maximum of peak 2 was observed at a slightly lower temperature for K(0)Na(0.71)Fe(2.63) (427°C) than for K(0.86)Na(0)Fe(2.69) (438°C), in agreement with results of Kubisz (1971) and Kashkay et al. (1975). X-ray diffraction analyses of samples heated at 475°C (peak 2) indicate that yavapaiite, $KFe(SO_4)_2$, is the major crystalline phase formed (Kulp and Adler, 1950; Kubisz, 1971).

XRD results for 475–550°C show diffraction peaks of hematite, indicating that peak 3 can be assigned to the crystalli-

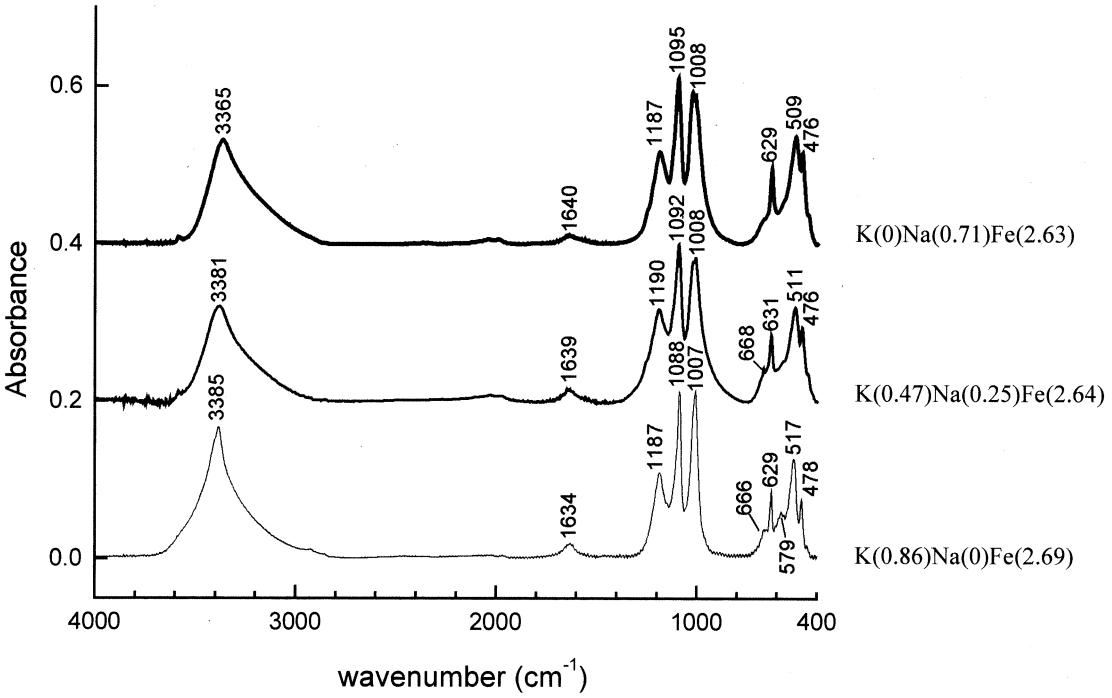

Fig. 5. FTIR spectra for jarosites K(0.86)Na(0)Fe(2.69), K(0.47)Na(0.25)Fe(2.64), and K(0)Na(0.71)Fe(2.63).

zation of α–Fe_2O_3 as already assumed by Kubisz (1971). These results show the breakdown of the jarosite structure through its dehydroxylation, which can be summarized, for the theoretical K-jarosite end-member, by the equation:

$$KFe_3(SO_4)_2(OH)_6 \rightarrow KFe(SO_4)_2 + Fe_2O_3 + 3H_2O \quad (1)$$

Because the deprotonation of hydronium-containing jarosites is generally observed at temperatures close to 400°C (Kubisz, 1971), this step is difficult to distinguish from the dehydroxylation process.

Despite the occurrence of an endothermic process (peak 4) and a weight loss near 5% in the range 550 to 700°C, the same crystalline phases are seen in the X-ray diffraction patterns corresponding to 590°C and 665°C. However, there is a noticeable increase of the $Fe_2O_3/KFe(SO_4)_2$ ratio. Kubisz (1971) reports that SO_3 loss generally occurs between 560°C and

Table 3. Thermodynamic cycle used for the determination of the enthalpy of formation of K-Na-H_3O jarosites.

	Reaction[a]	ΔH (kJ/mol)[b]
(1)	$(K_{1-x-y}, Na_y, (H_3O)_x)Fe_{3-z}(SO_4)_2(OH_{6-3z}, (H_2O)_{3z})$ (s, 298) → (1 − x − y)/2 K_2O (soln, 973) + y/2 Na_2O (soln, 973) + (3 − z)/2 Fe_2O_3 (soln, 973) + 2 SO_3 (soln, 973) + (6 + 3x + 3z)/2 H_2O (g, 973)	ΔH_{ds} (jarosite)
(2)	K_2SO_4 (s, 298) → K_2O (soln, 973) + SO_3 (soln, 973)	ΔH_{ds} (K_2SO_4)
(3)	Na_2SO_4 (s, 298) → Na_2O (soln, 973) + SO_3 (soln, 973)	ΔH_{ds} (Na_2SO_4)
(4)	2 K (s, 298) + S (s, 298) + 2 O_2 (g, 298) → K_2SO_4 (s, 298)	$\Delta H_f°$ (K_2SO_4)
(5)	2 Na (s, 298) + S (s, 298) + 2 O_2 (g, 298) → Na_2SO_4 (s, 298)	$\Delta H_f°$ (Na_2SO_4)
(6)	α-Fe_2O_3 (s, 298) → Fe_2O_3 (soln, 973)	ΔH_{ds} (αFe_2O_3)
(7)	2 Fe (s, 298) + 3/2 O_2 (g, 298) → αFe_2O_3 (s, 298)	$\Delta H_f°$ (Fe_2O_3)
(8)	SO_3 (g, 298) → SO_3 (soln, 973)	ΔH_{ds} ($SO_{3(g)}$)[c]
(9)	S (s, 298) + 3/2 O_2 (g, 298) → SO_3 (g, 298)	$\Delta H_f°$ ($SO_{3(g)}$)
(10)	H_2O (g, 298) → H_2O (g, 973)	ΔH_{hc} ($H_2O_{(g)}$)
(11)	H_2 (g, 298) + 1/2 O_2 (g, 298) → H_2O (g, 298)	$\Delta H_f°$ ($H_2O_{(g)}$)
Formation of jarosite:		
(12)	(1 − x − y) K (s, 298) + y Na (s, 298) + (3 − z) Fe (s, 298) + 2 S (s, 298) + (14 + x)/2 O_2 (g, 298) + (6 + 3x + 3z)/2 H_2 (g, 298) → $(K_{1-x-y}, Na_y, (H_3O)_x)Fe_{3-z}(SO_4)_2(OH_{6-3z}, (H_2O)_{3z})$ (s, 298)	$\Delta H_f°$ (jarosite)

$\Delta H_f°$ (jarosite) = $-\Delta H_1$ + (1 − x − y)/2 ΔH_2 + y/2 ΔH_3 + (1 − x − y)/2 ΔH_4 + y/2 ΔH_5 + (3 − z)/2 ΔH_6 + (3 − z)/2 ΔH_7 + (3 + x)/2 ΔH_8 + (3 + x)/2 ΔH_9 + (6 + 3x + 3z)/2 ΔH_{10} + (6 + 3x + 3z)/2 ΔH_{11}

[a] "s", "g", and "soln" are for "solid", "gas", and "in solution" (in sodium molybdate).
[b] ΔH_{ds}, $\Delta H_f°$, and ΔH_{hc} are respectively the drop solution enthalpy, standard enthalpy of formation, and heat content.
[c] ΔH_{ds} ($SO_{3(g)}$) as determined by Majzlan et al. (2002).

Table 4. Thermodynamic data for K- and Na-jarosite end-members.

	K-jarosite	Na-jarosite
Earlier estimates		
$\Delta H°_f$ (kJ/mol)	−3715.1[a]	−3673.1[a]
Maier-Kelley coefficients for heat capacity[e]:		
A ($J \cdot mol^{-1} \cdot K^{-1}$)	616.89[a]	616.39[a]
B (10^{-3} $J \cdot mol^{-1} \cdot K^{-2}$)	98.74[a]	91.21[a]
C (10^5 $J \cdot mol^{-1} \cdot K$)	−199.6[a]	−203.76[a]
$S°_{jarosite}$ ($J \cdot mol^{-1} \cdot K^{-1}$)	388.9[a]	382.4[a]
$S°_{elements}$ ($J \cdot mol^{-1} \cdot K^{-1}$)	2038.7[b]	2025.3[b]
$\Delta S°_f = S°_{jar.} - S°_{elem.}$ ($J \cdot mol^{-1} \cdot K^{-1}$)	−1648.8	−1642.9
$\Delta H°_f - T \cdot \Delta S°_f$ (kJ/mol) to be compared to $\Delta G°_f$ (kJ/mol)	−3223.5 −3309.8[c]	−3183.5 3256.7[d]
This work		
$\Delta H°_f$ (kJ/mol)	−3829.6	−3783.4
$\Delta H°_f - T \cdot \Delta S°_f$ (kJ/mol)	−3338.3	−3293.8
For sample K(0.86)Na(0)Fe(2.69):		
A ($J \cdot mol^{-1} \cdot K^{-1}$)	∼625	
B (10^{-3} $J \cdot mol^{-1} \cdot K^{-2}$)	∼110	
C (10^5 $J \cdot mol^{-1} \cdot K$)	∼−144	

[a] Estimation from data on alunite, hematite, and corundum (Stoffregen, 1993).
[b] Robie and Hemingway (1995).
[c] Baron and Palmer (1996).
[d] Kashkay et al. (1975).
[e] Maier-Kelley coefficient from the equation $Cp = A + B \cdot T + C/T^2$

900°C, and Alías and Girella (1968) showed that an endothermic peak accompanied this loss. Consequently, SO_3 loss could account for the endotherm observed at 550 to 700°C (Fig. 3). FTIR analysis indeed shows the presence of SO_2 (produced by decomposition of SO_3) in the gas phase at these temperatures by the appearance of two absorption bands at ca. 1150 and 1355 cm^{-1}, respectively assignable to asymmetric and symmetric stretching vibrations of gaseous sulfur dioxide. These considerations suggest that jarosite on the yavapaiite begins decomposing at these temperatures, probably through a reaction of the type:

$$KFe(SO_4)_2 \rightarrow 1/2\ Fe_2O_3 + 1/2\ K_2SO_4 + SO_3(g) \qquad (2)$$

Finally, the most intense peak seen by thermal analysis (peak 5) was observed near 750°C. X-ray diffraction analysis of a sample heated at 820°C shows the presence of hematite and K_2SO_4. These results are consistent with those previously published (Kulp and Adler, 1950; Kubisz, 1971) and indicate the complete thermal decomposition of yavapaiite $KFe(SO_4)_2$. The decomposition may be spread over a range of temperatures because of kinetic control and a distribution of grain sizes.

3.1.3. Fourier transform infrared spectroscopy (FTIR)

The FTIR spectra of the samples K(0.86)Na(0)Fe(2.69), K(0.47)Na(0.25)Fe(2.64), and K(0)Na(0.71)Fe(2.63) are shown in Figure 5. They are similar to those reported (Powers et al., 1975; Tuovinen and Carlson, 1979; Lazaroff et al., 1985; Arkhipenko et al., 1987; Baron and Palmer, 1996a).

The intense absorption observed in the region 2900 to 3700 cm^{-1} (Fig. 5) can be attributed to O-H stretching (ν_{OH}). This band shifts towards lower frequencies as the sodium content increases. This shift is probably due to an increase in energy of hydrogen bonds within the structure (Eagan and Bergeron, 1972; Powers et al., 1975). According to Hendricks (1937), sulfate oxygen atoms located on trigonal axes (along the "c" direction) of the unit cell are surrounded by three hydroxyl groups. Hendricks suggested that the hydrogen atoms are oriented in such a way as to bind to these oxygen atoms, thus

Table 5. Enthalpies of drop solution (ΔH_{ds}), of formation ($\Delta H°_f$) from the elements, and of mixing ($\Delta H°_{mixing}$(K, Na)).

	ΔH_{ds}[a] (kJ/mol)	$\Delta H°_{f,\ 298\ K}$ (kJ/mol)	$\Delta H°_{mixing}$(K, Na) (kJ/mol)
K_2SO_4	153.4 ± 1.8 (8)	−1437.7 ± 0.5[b]	
Na_2SO_4	155.7 ± 2.3 (6)	−1387.8 ± 0.4[b]	
α–Fe_2O_3	95.0 ± 1.8 (8)	−826.2 ± 1.3[b]	
$SO_{3(g)}$	−205.8 ± 3.7[c]	−395.7 ± 0.7[b]	
$H_2O_{(g)}$	—	−241.8 ± 0.0[b]	
Jarosites:			
$(H_3O)Fe_3(SO_4)_2(OH)_6$	466.3 ± 5.6 (5)	−3741.6 ± 8.3	
K(0.86)Na(0)Fe(2.69)	525.9 ± 6.7 (5)	−3803.2 ± 8.7	
K(0.72)Na(0)Fe(2.60)	504.1 ± 3.9 (7)	−3775.5 ± 6.8	
K(0.68)Na(0)Fe(2.58)	513.6 ± 5.6 (5)	−3783.6 ± 7.9	
K(0.58)Na(0)Fe(2.48)	502.6 ± 3.3 (7)	−3766.8 ± 6.5	
K(0.28)Na(0)Fe(2.52)	487.0 ± 5.2 (7)	−3748.1 ± 7.8	
K(0.63)Na(0.08)Fe(2.57)	522.4 ± 3.8 (8)	−3790.4 ± 6.7	−18 ± 6.3
K(0.59)Na(0.12)Fe(2.59)	500.2 ± 3.8 (5)	−3767.9 ± 6.7	3 ± 6.3
K(0.47)Na(0.25)Fe(2.64)	504.7 ± 3.7 (8)	−3771.2 ± 6.7	−5 ± 6.2
K(0.43)Na(0.29)Fe(2.66)	488.1 ± 2.2 (8)	−3754.4 ± 6.0	10 ± 5.5
K(0.33)Na(0.40)Fe(2.67)	483.2 ± 3.4 (8)	−3747.2 ± 6.6	12 ± 6.0
K(0)Na(0.82)Fe(2.91)	508.8 ± 5.3 (6)	−3772.9 ± 7.7	
K(0)Na(0.71)Fe(2.63)	471.2 ± 4.4 (14)	−3725.1 ± 7.1	
K(0)Na(0.68)Fe(2.83)	477.7 ± 5.0 (8)	−3739.9 ± 7.6	

[a] Enthalpies of drop solution, this work. Uncertainties are two standard deviations of the mean. Numbers in parentheses are the numbers of experiments performed.
[b] Enthalpies of formation from Robie and Hemingway (1995).
[c] Enthalpy of drop solution of $SO_{3(g)}$ determined by Majzlan et al. (2002).

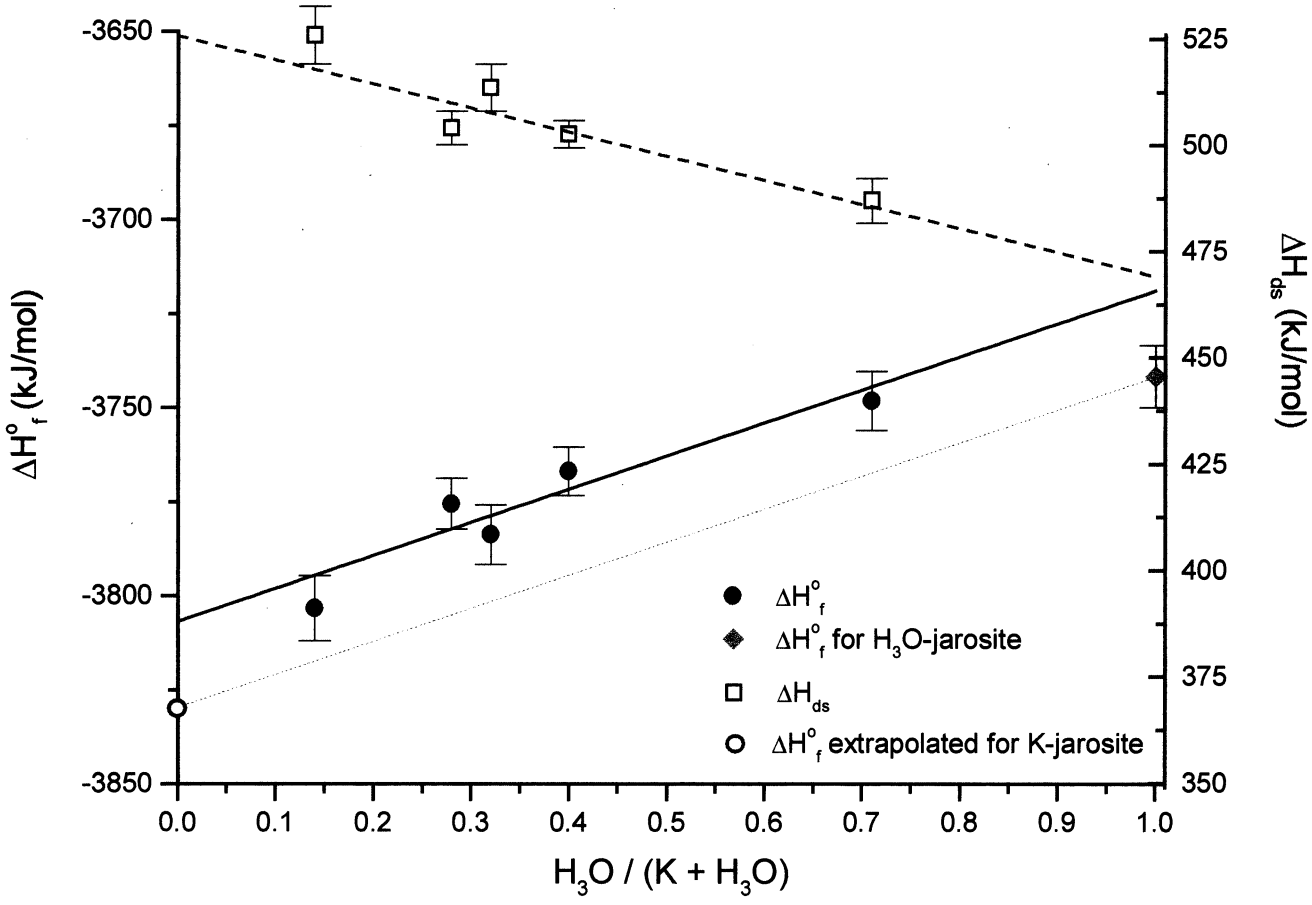

Fig. 6. Evolution of ΔH_{ds} and $\Delta H°_f$ for K-H_3O jarosites as a function of the hydronium content.

forming OH—OSO_3 hydrogen bonds, because no other ions (except for S^{6+}) are in their close vicinity. The unit cell parameter "c" decreases when the sodium content of the jarosite increases, whereas the parameter "a" remains almost constant (Table 1). Such a unidirectional contraction results in the decrease of some bond lengths, most probably including the OH—OSO_3 hydrogen bonds cited above (Hendricks, 1937). One can distinguish two vibrators around the hydrogen: O-H and H—OSO_3. Due to the contraction in the "c" direction, the bond length of the latter is likely to decrease, therefore strengthening the H—OSO_3 hydrogen bonds and, in turn, weakening the O-H vibrator in the hydroxyl groups (that are mostly responsible for the absorption at 2900 to 3700 cm^{-1}). The consequence of this is an overall decrease in frequency of the stretching vibration of the band observed at 2900 to 3700 cm^{-1} when the sodium content increases.

The band observed at 1634 to 1640 cm^{-1} (Fig. 5) was attributed to HOH deformation, in agreement with the results of Powers et al. (1975). Three intense absorption bands are observed near 1190, 1090, and 1008 cm^{-1} (Fig. 5). Arkhipenko et al. (1987) concluded that these absorptions are, respectively, due to the ν_3 (doublet) and ν_1 vibrations of sulfate species. However, Powers et al. (1975) attributed a band observed at 1003 cm^{-1} to OH deformation. These authors demonstrated

Table 6. Recommended thermodynamic data for H_3O-, K-, and Na-jarosite end-members.

at 298 K, 1 bar	K-jarosite	Na-jarosite	H_3O-jarosite
$\Delta H°_f$ (kJ/mol)	−3829.6 ± 8.3[a]	−3783.4 ± 8.3[a]	−3741.6 ± 8.3[a]
$S°$ ($J \cdot mol^{-1} \cdot K^{-1}$)	388.9[b]	382.4[b]	563.5[e]
$\Delta S°_f$ ($J \cdot mol^{-1} \cdot K^{-1}$)	−1648.8	−1642.9	−1709.1[e]
$\Delta G°_f$ (kJ/mol)	−3309.8 ± 1.7[c]	−3256.7 ± 8.4[d]	−3232.3 ± 8.4[d]

[a] This work.
[b] Calculated by Stoffregen (1993).
[c] Baron and Palmer (1996).
[d] Kashkay et al. (1975).
[e] Estimated in this work from $\Delta H°_f$ and $\Delta G°_f$ values.

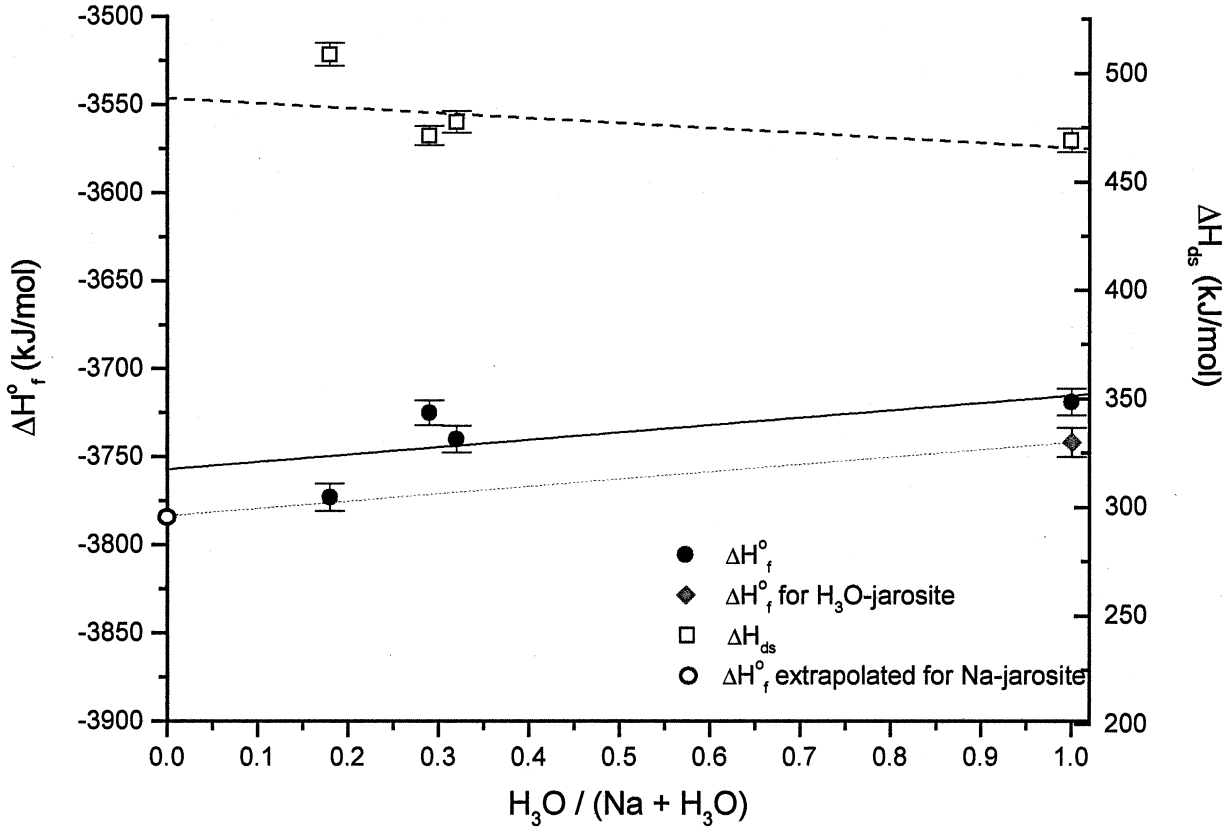

Fig. 7. Evolution of ΔH_{ds} and $\Delta H°_f$ for Na-H_3O jarosites as a function of the hydronium content.

that this band was shifted to 761 cm^{-1} for a deuterated K-jarosite, whereas bands observed at 1181 and 1080 cm^{-1} were not modified by D-H substitution. This observation supports the assignment of the band observed near 1008 cm^{-1} to OH deformations rather than $\nu_1(SO_4)$. Several absorptions were also observed in the 400 to 1000 cm^{-1} region. The absorption close to 630 cm^{-1}, as well as the weak shoulder observed near 670 cm^{-1}, can be attributed to the ν_4 vibration mode of sulfate (Arkhipenko et al., 1987). The $\nu_4(SO_4)$ doublet is distinguishable by IR due to the decrease in symmetry of the sulfate species in the jarosite structure. Note that the vibrations $\nu_1(SO_4)$ and $\nu_2(SO_4)$ could not be seen here, most probably due to overlap with other nearby intense absorptions. Powers et al. (1975) attributed IR bands observed near 505 and 470 cm^{-1} to vibrations of FeO_6 coordination octahedra, and a similar origin is likely for the bands observed at 510 and 480 cm^{-1} (Fig. 5).

3.2. Calorimetry

3.2.1. Thermodynamic issues

As mentioned above, very few reliable thermodynamic data are available for jarosites and, to our knowledge, such data are nonexistent for K-Na-H_3O jarosite solid solutions. The latest values recommended (Stoffregen et al., 2000) for the enthalpy of formation, entropy, and heat capacity of potassium jarosite and natrojarosite was derived from approximations and estimations (Stoffregen, 1993) rather than direct determinations. As shown in Table 4, the results are not consistent with the latest measurements of the free energy of formation because we see only poor agreement with the equation $\Delta G°_f = \Delta H°_f - T.\Delta S°_f$. The first point to clarify is thus the origin of such inconsistencies.

The entropy of K-jarosite can be used to calculate ΔS_r, corresponding to the hypothetical reaction:

$$KFe_3(SO_4)_2(OH)_6 + 3/2\ Al_2O_{3,\ corundum} \rightarrow KAl_3(SO_4)_2(OH)_6 + 3/2\ Fe_2O_{3,\ hematite} \quad (3)$$

By using published data for corundum, hematite, and alunite (Robie and Hemingway, 1995) and the value for the entropy of K-jarosite given by Stoffregen (1993), ΔS_r is relatively small (-13.15 $J.mol^{-1}.K^{-1}$). This is indeed expected for a reaction involving only solid phases (small volume change). The heat capacity (C_p) of the jarosite K(0.86)Na(0)Fe(2.69) was determined in this work from DSC. The corresponding Maier-Kelley coefficients A, B, and C (Maier and Kelley, 1932) were fitted by least squares refinement using the equation $Cp = A + BT + CT^{-2}$. The coefficients obtained (Table 4) are similar to those approximated by Stoffregen (1993).

The free energy of formation ($\Delta G°_f$) that is recommended for K-jarosite has been determined recently (Baron and Palmer, 1996a) from dissolution experiments carried out under controlled experimental conditions. The samples used by these authors were well characterized, and the approach to equilibrium in solution was well documented. Thus, these values are likely to be reliable.

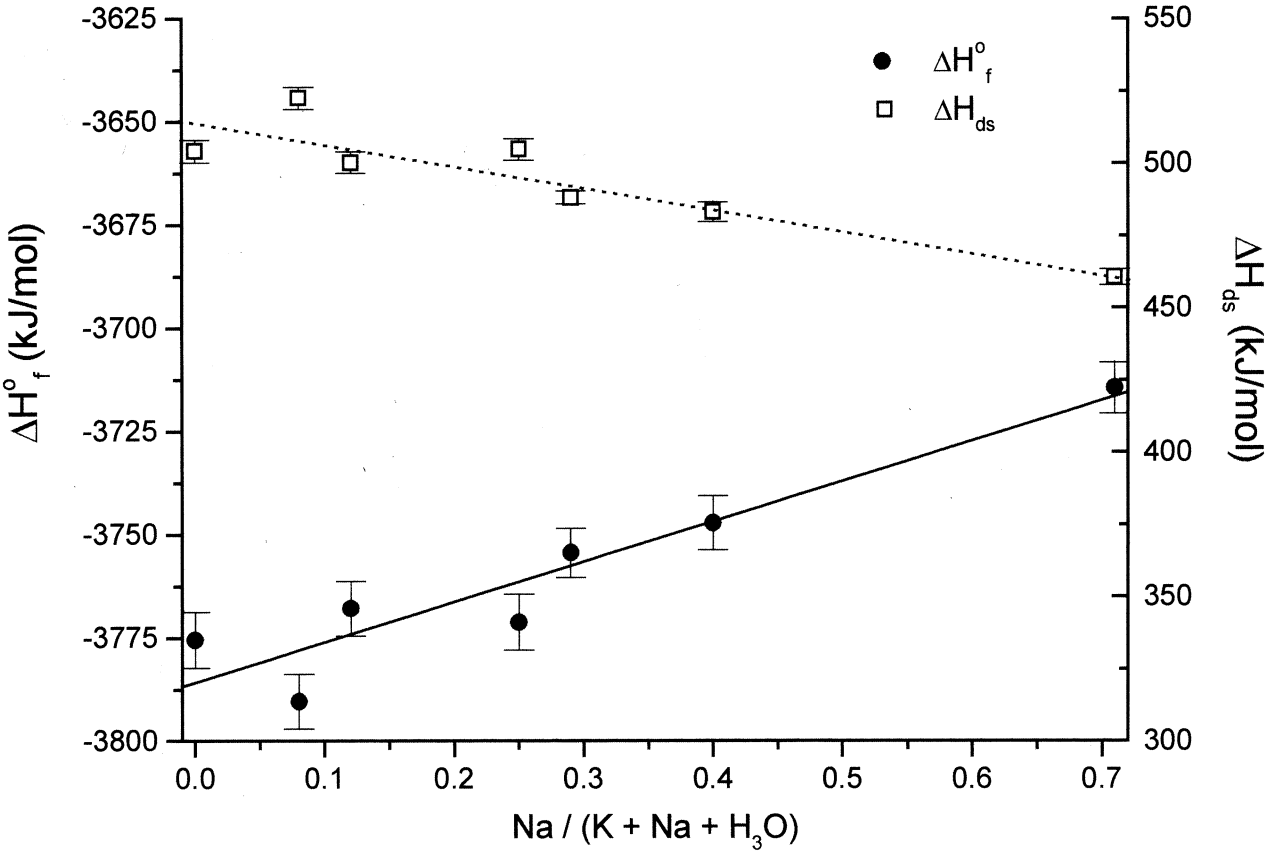

Fig. 8. Evolution of ΔH_{ds} and $\Delta H°_f$ for ($K_{0.7-y}$, Na_y, $(H_3O)_{0.3}$) jarosites as a function of the sodium content.

3.2.2. *Thermodynamic cycle*

Considering the above, the inconsistencies existing among the recommended values for $\Delta G°_f$, $\Delta H°_f$, and S° most probably arise mainly from poor estimates of enthalpies of formation, $\Delta H°_f$. Enthalpies of formation have been determined in this work from high-temperature oxide melt calorimetry using an appropriate thermodynamic cycle.

The enthalpy of formation from the elements of K-H_3O, Na-H_3O, and K-Na-H_3O jarosites was based on the thermodynamic cycle reported in Table 5. The enthalpy of reaction (10), ΔH_{hc} ($H_2O_{(g)}$), is the heat content of gaseous water. Reaction (8) corresponds to the drop solution of gaseous SO_3 into sodium molybdate. The enthalpy of this hypothetical reaction ($\Delta H_{ds} = -205.8 \pm 3.7$ kJ.mol^{-1}) has been determined recently by Majzlan et al. (2002) from drop solution calorimetric experiments using various sulfate/oxide and sulfate/carbonate pairs.

Table 7. Enthalpies of formation ($\Delta H°_f$) and dehydration (ΔH_{dehy}) for some jarosites.

Initial jarosite	Dehydrated jarosite	
	$\Delta H°_f$ (kJ/mol)	ΔH_{dehy}[a] (kJ/mol)
K(0.72)Na(0)Fe(2.60)	−3428.5 ± 6.6	56.9 ± 7.4
K(0.28)Na(0)Fe(2.52)	−3370.8 ± 6.4	29.1 ± 6.2
K(0.59)Na(0.12)Fe(2.59)	−3434.3 ± 5.9	36.2 ± 5.8
K(0.43)Na(0.29)Fe(2.66)	−3470.6 ± 6.2	37.2 ± 4.8
K(0)Na(0.71)Fe(2.63)	−3415.9 ± 6.3	30.1 ± 5.9

[a] Enthalpy of dehydration at the reference conditions 1 bar, 298 K, and gaseous H_2O.

3.2.3. *Enthalpy of formation*

K-H_3O jarosites. The evolution of the enthalpy of drop solution (ΔH_{ds}) and formation ($\Delta H°_f$) for K-H_3O jarosites is plotted in Figure 6 as a function of the hydronium mole fraction in A-sites determined from microprobe results. The corresponding data are given in Table 5. ΔH_{ds} and $\Delta H°_f$ vary linearly with the hydronium content. The scatter is mostly due to slightly different iron contents. Such linear variations are indicative of solid solutions near ideality. By following this linear trend, the enthalpy of formation extrapolated to $H_3O/(K + H_3O) = 1$ is –3718.8 kJ.mol^{-1}. However, the K-H_3O jarosite samples prepared here contain iron vacancies, with their iron content close to 2.60 to 2.70 mol (rather than 3 mol) per unit formula unit. Consequently, a correction for the presence of iron vacancies has to be made to evaluate the enthalpy of formation of stoichiometric K-H_3O jarosites. For that purpose, we synthesized hydronium jarosite hydrothermally. Electron probe microanalyses showed that the chemical composition of this sample corresponded to the end-member $(H_3O)Fe_3(SO_4)_2(OH)_6$.

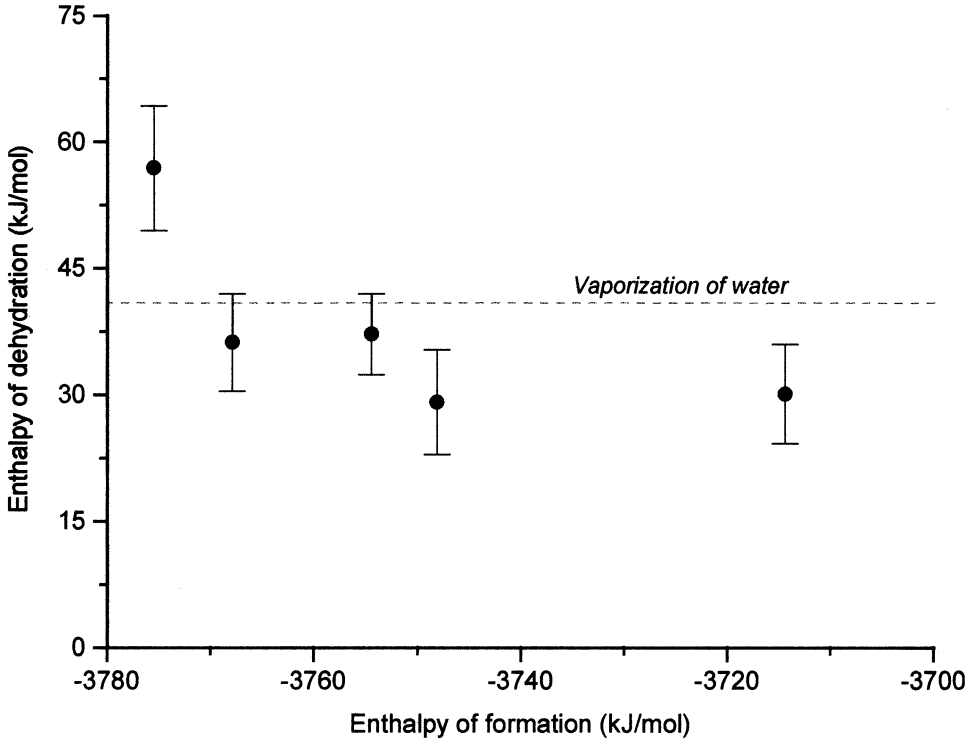

Fig. 9. Evolution of ΔH_{dehy} vs. $\Delta H°_f$ for some jarosites.

The enthalpy of drop solution of this H_3O-jarosite was then determined (Table 5), leading to the enthalpy of formation $\Delta H°_f = -3741.6 \pm 8.3$ kJ.mol^{-1}. This point has been added in Figure 6. A new line could then be drawn from that point (dotted line), corresponding to the enthalpy of formation of stoichiometric K-H_3O jarosites. Extrapolation to $H_3O/(K + H_3O) = 0$ gave the enthalpy of formation of the K-jarosite end-member $KFe_3(SO_4)_2(OH)_6$: $\Delta H°_f = -3829.6 \pm 8.3$ kJ · mol^{-1}. Using the entropy of K-jarosite estimated by Stoffregen (1993), $S° \approx 388.9$ J.mol^{-1}.K^{-1}. The free energy $\Delta G°_f = -3338.3$ kJ.mol^{-1}. The error on that value is difficult to calculate because Stoffregen (1993) did not give errors on the entropy value. This $\Delta G°_f$ is relatively close to the experimental value (-3309.8 kJ.mol^{-1}) obtained experimentally by Baron and Palmer (1996a). Taking into account the uncertainty in S°, the difference of 1% (30 kJ.mol^{-1}) between these two values seems reasonable.

Na-H_3O jarosites. A similar approach was used for Na-H_3O jarosites. Again, we observed a linear variation of ΔH_{ds} and $\Delta H°_f$ as a function of the hydronium content (Fig. 7). By taking into account the correction for iron vacancies as above, the extrapolation to the stoichiometric end-member Na-jarosite gave $\Delta H°_f = -3783.4 \pm 8.3$ kJ.mol^{-1}. By using the entropy estimated by Stoffregen (1993) for natrojarosite, the corresponding free energy for end-member Na-jarosite is $\Delta G°_f = -3293.8 \pm 8.3$ kJ.mol^{-1} which is, again, relatively close (within 1%) to the value (-3256.7 kJ.mol^{-1}) reported by Kashkay et al. (1975).

K-Na-H_3O jarosites. The enthalpies of drop solution and formation of (K, Na, $(H_3O)_{0.30}$) jarosites were determined (Table 5) and plotted vs. the sodium content (Fig. 8). A linear relationship between $\Delta H°_f$ and the substitution ratio in A-sites is seen. $\Delta H°_f$ increases with increasing sodium-for-potassium substitution.

The enthalpy of mixing ΔH_{mixing}(K/Na) for these K-Na-H_3O jarosites can be defined as the enthalpy of the reaction:

$$\frac{0.7 - y}{0.7}(K_{0.7}(H_3O)_{0.3})\text{jarosite} + \frac{y}{0.7}(Na_{0.7}(H_3O)_{0.3})\text{jarosite} \rightarrow (K_{0.7-y}Na_y(H_3O)_{0.3})\text{jarosite} \quad (4)$$

In all cases, ΔH_{mixing}(K/Na) is essentially zero (Table 5). This is an additional point suggesting that these solid solutions are indeed close to ideal.

Based on the above considerations and results, we recommend thermodynamic data for the end-members K-, Na-, and H_3O-jarosites as indicated in Table 6. Entropy values from Stoffregen (1993) should be verified experimentally in the future.

Dehydrated jarosites. The enthalpies of formation of dehydrated jarosites were determined by drop solution calorimetry (Table 7). The enthalpy of dehydration, ΔH_{dehy}, can be defined as the enthalpy change accompanying, at 1 bar and 25°C, the reaction:

$$\text{Jarosite}_{(s,\,298)} \rightarrow \text{Dehydrated jarosite}_{(s,\,298)} + n\,H_2O_{(g,\,298)} \quad (5)$$

where "n" is the number of molecules of "additional" water per unit formula (see Table 2). Gaseous water rather than liquid was chosen here as a convenient reference state because in practice this dehydration generally takes place at temperatures

above 100°C. Values of ΔH_{dehy} then can be calculated from (Table 5)

$$\Delta H_{dehy} = \Delta H_{ds}(\text{jarosite}) - \Delta H_{ds}(\text{dehydrated jarosite}) - n(H_{700°C} - H_{25°C})\,(H_2O, \text{gas}) \quad (6)$$

ΔH_{dehy} values are given in Table 7 and shown in Figure 9 as a function of the enthalpy of formation of the initial jarosite. The molar enthalpies of dehydration are the same, within experimental error, to the molar enthalpy of vaporization of water (40.9 $kJ.mol^{-1}$, Robie and Hemingway, 1995), although the point corresponding to the sample K(0.72)Na(0)Fe(2.60) is slightly higher. This observation indicates that this "additional" water is not strongly bound, which agrees with the DSC data in which this water loss is observed at low temperature (180–300°C) (Fig. 3).

Stability field diagrams (Brown, 1971; Van Breemen and Harmsen, 1975; Alpers et al., 1989; Stahl et al., 1993; Stoffregen, 1993; and others) were based on the solubility products K_{SP} of the phases involved. The overall constant of the equilibrium between two phases (K_{eq}) is directly linked to the change in free energy $\Delta G°$ through the equation $\Delta G° = -RTlnK_{eq}$, and values of $\Delta G°_f$ considered by these authors for K-jarosite (ca. –3318 $kJ.mol^{-1}$) were close to those determined by Baron and Palmer (1996a). The values of $\Delta G°$ recommended here, based on calorimetric data, are similar, so that such potential-pH diagrams do not require modification after the present work. The calorimetric data suggest that equilibrium was indeed attained in the solubility studies on which these diagrams are based.

The present work recommends values for enthalpy, entropy, and free energy of the three end-member jarosites (Na^+, K^+, H_3O^+). It suggests ideal mixing among these end-members. It shows that the "additional" water commonly present in jarosites is only loosely bound. This work is a starting point for dealing with even more complex natural systems, for example, those showing Fe^{3+}–Al^{3+} substitution (jarosite–alunite) or S^{6+}–Cr^{6+} substitution.

Acknowledgments—The authors thank Juraj Majzlan, John Neil, and Eric Moloy for interesting discussions and comments; and Sarah Roeske and Peter Schiffman for their assistance in electron probe microanalysis. This work was supported by the U.S. Department of Energy (grant DE-FG0397SF 14749).

Associate editor: B. Mysen

REFERENCES

Alías L. J. and Girella F. (1968) Estudio por anαlisis térmico diferencial de soluciones sólidas y mezclas de jarosita y alunita. *Estudios Geologicos* **24,** 79–83.

Alpers C. N., Nordstrom D. K., and Ball J. W. (1989) Solubility of jarosite solid solutions precipitated from acid mine waters, Iron Mountain, California, U.S.A. *Sci. Géol. Bull.* **42,** 281–298.

Alpers C. N., Rye R. O., Nordstrom D. K., White L. D., and Bi-Shia King. (1992) Chemical, crystallographic and stable isotopic properties of alunite and jarosite from acid-hypersaline Australian lakes. *Chem. Geol.* **96,** 203–226.

Arehart G. B., O'Neil J. R. (1993) D/H ratios of supergene alunite as an indicator of paleoclimate in continental settings. *Climate Change in Continental Isotopic Records, Geophysical Monograph.* **78,** 277–284.

Arkhipenko D. K., Deviatkina E. T., and Palchik H. A. (1987) Kristallokhimicheskiye osobennosti sinteticheskikh yarozitov (in Russian). *Trudy Instituta Geologii I Geofiziki* **653,** 31–70.

Arregui V., Gordon A. R., and Steintveit G. (1979) The jarosite process: Past, present and future. In *Lead-Zinc-Tin '80* (eds. J. M. Cigan, T. S. Mackey, and T. O'Keefe), pp. 97–123. The Mineralogical Society of AIME, Warrendale, PA.

Balic-Zunic T., Moelo Y., Loncar Z., and Micheelsen H. (1994) Dorallcharite, $(Tl_{0.8}K_{0\cdot2})$Fe3(SO_4)2(OH)6: A new member of the jarosite-alunite family. *Eur. J. Mineral.* **6,** 255–263.

Baron D. and Palmer C. D. (1996a) Solubility of jarosite at 4–35 °C. *Geochim. Cosmochim. Acta* **60,** 185–195.

Baron D. and Palmer C. D. (1996b) Solubility of $KFe_3(CrO_4)_2(OH)_6$ at 4 to 35 °C. *Geochim. Cosmochim. Acta* **60,** 3815–3824.

Breidenstein B., Schlueter J., and Gebhard G. (1992) On beaverite: New occurrence, chemical data, and crystal structure. *Neues Jahrbuch fuer Mineralogie Monatshefte* **5,** 213–220.

Brophy G. P., Scott E. S., and Snellgrove R. A. (1962) Sulfate studies II: Solid solution between alunite and jarosite. *Am. Miner.* **22,** 773–784.

Brophy G. P. and Sheridan M. F. (1965) Sulfate studies IV: The jarosite-natrojarosite-hydronium jarosite solid solution series. *Am. Miner.* **50,** 1595–1607.

Brown J. B. (1970) A chemical study of some synthetic potassium-hydronium jarosites. *Can. Mineral.* **10,** 696–703.

Brown J. B. (1971) Jarosite-goethite stabilities at 25°C, 1 atm. *Mineral. Deposita* **6,** 245–252.

Burns R. G. (1987) Gossans on Mars; spectral features attributed to jarosites. NASA Technical Memorandum Reports of the Planetary Geology and Geophysics Program, 89810. 176–177.

Dutrizac J. E. and Kaiman S. (1976) Synthesis and properties of jarosite-type compounds. *Can. Mineral.* **14,** 151–158.

Dutrizac J. E. (1979) The physical chemistry of iron precipitation in the zinc industry. In *Lead-Zinc-Tin '80* (eds. J. M. Cigan, T. S. Mackey, and T. J. O'Keefe), pp. 532–564. The Mineralogical Society of AIME, Warrendale, PA.

Dutrizac J. E. (1984) The behavior of impurities during jarosite precipitation. In *Hydrometallurgical Process Fundamentals* (ed. R. G. Bautista), pp. 125–169. Plenum.

Dutrizac J. E., and Jambor J. L. (1984) Formation and characterization of argentojarosite and plumbojarosite and their relevance to metallurgical processing. *Proceedings of the Second International Congress on Applied Mineralogy in the Minerals Industry*, Los Angeles, California, pp. 507–530. The Mineralogical Society of AIME, Warrendale, PA.

Dutrizac J. E., Jambor J. L., and Chen T. T. (1987) The behaviour of arsenic during jarosite precipitation: Reactions at 150°C and the mechanism of arsenic precipitation. *Can. Metall. Quarterly* **26,** 103–115.

Eagan R. J. and Bergeron C. G. (1972) Determination of water in lead borate glasses. *J. Am. Ceram. Soc.* **55,** 53–54.

Helgeson H. C., Delany J. M., Nesbitt H. W., and Bird D. K. (1978) Summary and critique of the thermodynamic of rock-forming minerals. *Am. J. Sci.* **278A,** 1–229.

Hendricks S. B. (1937) The crystal structure of alunite and the jarosites. *Am. Miner.* **22,** 773–784.

Herbert R. B. (1997) Properties of goethite and jarosite precipitated from acidic ground water, Dalarna, Sweden. *Clays and Clay Miner.* **45,** 261–273.

Jambor J. L., Owens D. R., Grice J. D., and Feinglos M. N. (1996) Gallobeudantite, $PbGa_3(AsO_4, SO_4)_2(OH)_6$, a new mineral species from Tsumeb, Namibia, and associated new gallium analogues of the alunite-jarosite family. *Canad. Miner.* **34,** 1305–1315.

Kashkay C. M., Borovskaya Y. B., and Babazade M. A. (1975) Determination of $\Delta G°_{f,\ 298}$ of synthetic jarosite and its sulfate analogues. *Geochem. Intl. 1975*, 115–121, translated from *Geokhimiya* **5,** 778–784.

Kay P. T., Wendlandt R. F., Williamson D. L., and McGrew R. A. (1996) Widespread use of natrojarosite as pigment by prehistoric Native American cultures of the Four Corners region, southwestern U.S.A. *Geological Society of America, 28th Ann. Meeting,* **28,** 88.

Kubisz J. (1964) A study on minerals of the alunite-jarosite group. *Polska. Akad. Nauk. Prace Geol.* **22,** 1–90.

Kubisz J. (1970) Studies on synthetic alkali-hydronium jarosites. I. Synthesis of jarosite and natrojarosite. *Mineralogia Polonica* **1,** 47–57.

Kubisz J. (1971) Studies on synthetic alkali-hydronium jarosites. II: Thermal investigations. *Mineralogia Polonica* **2,** 51–59.

Kulp J. L. and Adler H. H. (1950) Thermal study of jarosite. *Am. J. Sci.* **248,** 475–487.

Lazaroff N., Melanson L., Lewis E., Santoro N., and Pueschel C. (1985) Scanning electron microscopy and infrared spectroscopy of iron sediments formed by thiobacillus ferrooxidans. *Geomicrobiol. J.* **4,** 231–267.

Lengauer C. L., Giester G., and Irran E. (1994) $KCr_3(SO_4)_2(OH)_6$: Synthesis, characterization, powder diffraction data, and structure refinement by the Rietveld technique and a compilation of alunite-type compounds. *Powd. Diffract.* **9,** 265–271.

Maier C. G. and Kelley K. K. (1932) An equation for the representation of high-temperature heat content data. *J. Am. Chem. Soc.* **54,** 3243–3246.

Majzlan J., Navrotsky A., and Neil J. M. (2002) Energetics of anhydrite, barite, celestine, and anglesite: A high-temperature and differential scanning calorimetry study. *Geochim. Cosmochim. Acta* **66,** 1839–1850.

Menchetti S. and Sabelli C. (1976) Crystal chemistry of the alunite series; crystal structure refinement of alunite and synthetic jarosite. *Neues Jahrbuch fuer Mineralogie. Monatshefte* **9,** 406–417.

Ming D. W., Golden D. C., Gooding J. L., Morris R. V., Thompson D. R., Bell J. F. (1996) Mineralogical and thermal properties of jarositic tephra on Mauna Kea, Hawaii; implications for the sulfur mineralogy on Mars. *Lunar and Planetary Science Conference*, **27-2,** 883–884. Lunar and Planetary Science Conference, Houston, TX.

Mymrin V. and Vaamonde A. V. (1999) New construction materials from Spanish jarosite processing wastes. *Miner. Eng.* **12,** 1399–1402.

Navrotsky A. (1977) Progress and new directions in high temperature calorimetry. *Phys. Chem. Miner.* **2,** 89–104.

Navrotsky A., Rapp R. P., Smelik E., Burnley P., Circone S., Chai L., and Bose K. (1994) The behavior of H_2O and CO_2 in high-temperature lead borate solution calorimetry of volatile-bearing phases. *Am. Miner.* **79,** 1099–1109.

Navrotsky A. (1997) Progress and new directions in high temperature calorimetry revisited. *Phys. Chem. Miner.* **24,** 222–241.

Parker R. L. (1954) Alunitic alteration at Marysvale, Utah. Thesis, Columbia University.

Parker R. L. (1962) Isomorphous substitution in natural and synthetic alunite. *Am. Miner.* **47,** 127–136.

Powers D. A., Rossman G. R., Schugar H. J., and Gray H. B. (1975) Magnetic behavior and infrared spectra of jarosite, basic iron sulfate and their chromate analogs. *J. Sol. Stat. Chem.* **13,** 1–13.

Ripmeester J. A., Ratcliffe C. I., Dutrizac J. E., and Jambor J. L. (1986) Hydronium in the alunite-jarosite group. *Can. Miner.* **22,** 773–784.

Robie R. A., Hemingway B. S. (1995) Thermodynamic properties of minerals and related substances at 298.15K and 1bar (10^5 Pascals) pressure and at higher temperatures. *U.S. Geological Survey Bull.* **2131**.

Rye R. O., Bethke P. M., Lanphere M. A., Steven T. A. (1993) Age and stable isotope systematics of supergene alunite and jarosite from the Creed mining district, Colorado: Implications for supergene processes and neogene geomorphic evolution and climate of the southern Rocky Mountains. *Geological Society of America, 1993 Ann. Meeting.* **25,** 274.

Shannon R. D. and Prewitt C. T. (1969) Effective ionic radii in oxides and fluorides. *Acta Cryst.* **B25,** 925–946.

Shannon R. D. (1976) Revised effective ionic radii and systematic studies of interatomic distances in halides and chalcogenides. *Acta Cryst.* **A32,** 752–767.

Stahl R. S., Fanning D. S., and James B. R. (1993) Goethite and jarosite precipitation from ferrous sulfate solutions. *Soil Sci. Soc. Am. J.* **57,** 280–282.

Stoffregen R. E. and Alpers C. N. (1992) Observations on the unit-cell dimensions, H_2O contents and δD values of natural and synthetic alunite. *Am. Miner.* **77,** 1092–1098.

Stoffregen R. E. (1993) Stability of jarosite and natrojarosite at 150–250 °C. *Geochim. Cosmochim. Acta* **57,** 2417–2429.

Stoffregen R. E., Alpers C. N., and Jambor J. L. (2000) Alunite-jarosite crystallography, thermodynamics and geochronology. *Rev. Mineral. Geochem.* **40,** 453–479.

Tuovinen O. H. and Carlson L. (1979) Jarosite in cultures of iron-oxidizing thiobacilli. *Geomicrobiol. J.* **1,** 205–210.

Van Breemen N. and Harmsen K. (1975) Translocation of iron in acid sulfate soils. I. Soil morphology and the chemistry and mineralogy of iron in a chronosequence of acid sulfate soils. *Soil Sci. Soc. Am. Proc.* **39,** 1140–1147.

Vasconcelos P. M., Brimhall G. H., Becker T. A., and Renne P. R. (1994) ^{40}Ar and ^{39}Ar analysis of supergene jarosite and alunite: Implications to the paleoweathering history of the western U.S.A. and west Africa. *Geochim. Cosmochim. Acta* **58-1,** 401–420.

Vlek P. L. G., Blom T. G. M., Beek J., and Lindsay W. L. (1974) Determination of the solubility product of various iron hydroxides and jarosite by the chelation method. *Soil Sci. Soc. Am. Proc.* **38,** 429–432.

Zotov A. V., Mironova G. D., and Rusinov V. L. (1973) Determination of $\Delta G°_f$ of jarosite synthesized from a natural solution. *Geochem. Intl.* **5,** 577–582.